Hindawi
Journal of Function Spaces
Volume 2022, Article ID 2297866, 16 pages
https://doi.org/10.1155/2022/2297866

Research Article

New Fractal Soliton Solutions and Sensitivity Visualization for Double-Chain DNA Model

Zara Hassan,[1] Nauman Raza,[1] Abdel-Haleem Abdel-Aty,[2,3] Mohammed Zakarya,[4] Riaz Ur Rahman,[5] Adeela Yasmeen,[1] Abdisalam Hassan Muse,[6] and Emad E. Mahmoud[7]

[1]*Department of Mathematics, University of the Punjab, Quaid-e-Azam Campus, Lahore, Pakistan*
[2]*Department of Physics, College of Sciences, University of Bisha, PO Box 344, Bisha 61922, Saudi Arabia*
[3]*Physics Department, Faculty of Science, Al-Azhar University, Assiut 71524, Egypt*
[4]*Department of Mathematics, College of Science, King Khalid University, P.O. Box 9004, Abha 61413, Saudi Arabia*
[5]*Department of Mathematics, University of Management and Technology, 54770 Lahore, Pakistan*
[6]*Department of Mathematics (Statistics Option) Program, Pan African University, Institute of Basic Science, Technology and Innovation (PAUSTI), Nairobi 6200-00200, Kenya*
[7]*Department of Mathematics and Statistics, College of Science, Taif University, PO Box 11099, Taif 21944, Saudi Arabia*

Correspondence should be addressed to Abdel-Haleem Abdel-Aty; amabdelaty@ub.edu.sa
and Abdisalam Hassan Muse; muse.abdisalam@students.jkuat.ac.ke

Received 13 June 2022; Revised 8 July 2022; Accepted 26 July 2022; Published 25 August 2022

Academic Editor: Yusuf Gurefe

This article discusses dynamics of the fractal double-chain deoxyribonucleic acid model. This structure contains two long elastic homogeneous strands that serve as two polynucleotide chains of deoxyribonucleic acid molecules, bounded by an elastic membrane indicating hydrogen bonds between the base pairs of two chains. The semi-inverse variational principle and auxiliary equation method are employed to extricate soliton solutions. The collection of retrieved exact solutions includes bright, dark, periodic, and other solitons. The constraint conditions emerge naturally which ensure the presence of these solutions. Additionally, 2D and 3D graphs showing the impact of fractals on solutions are included. These plots use appropriate parameter values. Furthermore, sensitivity analysis of the considered model is also acknowledged. The outcomes reveal that these techniques are reliable, effective, and applicable to various biological systems.

1. Introduction

Deoxyribonucleic acid (DNA) is an interesting nonlinear model of biological sciences [1, 2]. Since it is needed for protein-coding, inheritance, and genetic instruction manual for life, it contains instructions for cell growth, reproduction, and death of a human. DNA molecules are the foundation of life so their dynamics are one of the interesting problems in biophysics. Researchers have been studying this structure during the last decades [3, 4]. The study of DNA mechanism predicts the presence of significant nonlinear structures. It has been established that localized waves are caused by nonlinearity and these waves are fascinating because they can transmit power without causing power loss [5–7].

Nonlinear partial differential equations (NLPDEs) have been considered for studying several nonlinear physical phenomena. Many physicists and mathematicians have worked hard to develop further precise alternatives to NLPDEs for a better understanding of these processes. Therefore, exact solutions of NLPDEs are essential for exploring physical explanations and qualitative aspects of different mechanisms [8–18]. These solutions demonstrate the dynamics of several nonlinear complex models symbolically and physically. Numerous methods were implemented to attain exact and wave solutions of the nonlinear governing model [19–26].

This paper introduces the fractal double-chain DNA model to scrutinize the double-helix structure. Fractal calculus has been a flourishing subject of biology, mathematics, and physics

because it deals with the modeling of distinct nonlinear procedures [27–34]. Since the fractal model covers many powerful properties, which the traditional system fails to explain. The field of biophysics greatly benefits from a unique class of solitary wave solutions referred to as solitons of proposed problems [3]. Wave packets known as solitons propagate at a constant pace and maintain their shape despite nonlinearities and dispersion [35–43]. Semi-inverse scheme and auxiliary equation method (AEM) are two effective techniques implemented to derive a set of solitons in this manuscript.

The Ritz-like approach linked with the variational principle termed as He's semi-inverse variational method [44] is applied to attain the bright solitons of fractal DNA model which may aid biologists to comprehend its physical significance. An effective and straightforward algebraic method for finding soliton solutions is the semi-inverse scheme [45]. Many authors contributed to develop this technique to analyze fractal models in distinct scientific fields [33, 46, 47]. Another method adopted here is AEM that retrieves dark, periodic, bright, and other shaped solitons. This reliable strategy is employed to obtain dual-mode solutions of various equations found in literature [48, 49]. It is the generalization of many existing techniques. By using various values of the parameters and fractal dimension, the nonlinear dynamics of DNA strands can be addressed. The sensitivity analysis assesses how different uncertainties affect the overall level of uncertainty in a mathematical model. Specific boundaries that are dependent on one or more parameters have been applied using this technique.

The rest of the article is organize as follows: The governing model is included in Section 2. In section 3, soliton solutions are extracted along with geometrical analysis by employing semi-inverse method. Section 4 comprises solitons obtained via AEM with graphs. Section 5 of the report discusses the findings. Section 6 provides a sensitivity analysis of the suggested system. The article's conclusion is provided in Section 7.

2. Governing System

Consider the following two general nonlinear dynamical equations which describe double-chain model of DNA:

$$u_{\tau\tau} - \beta_1^2 u_{xx} = \sigma_1 u + \xi_1 uv + \eta_1 u^3 + \alpha_1 uv^2, \tag{1}$$

$$v_{\tau\tau} - \beta_2^2 v_{xx} = \sigma_2 v + \xi_2 u^2 + \eta_2 u^2 v + \alpha_2 v^3 + a, \tag{2}$$

where u is the difference between the top and bottom strands' longitudinal displacements, i.e., the deviations of the bases from their equilibrium positions along the direction of the phosphodiester bridge, which joins the two bases of the same strands, v is the difference between the bottom and top strands' transverse displacements, i.e., the bases displacement from its equilibrium point with the pathway of hydrogen bond which joins two bases of base pair where

$$\beta_1 = \pm\frac{G}{\nu}, \beta_2 = \pm\frac{H}{\nu}, \sigma_1 = -\frac{2\eta}{\nu bh}(h - m_o), \sigma_2 = -\frac{2\eta}{\nu b}, \xi_1 = 2\xi_2 = \frac{2\sqrt{2}\eta m_o}{\nu bh^2},$$
$$\eta_1 = \eta_2 = -\frac{2\eta m_o}{\nu bh^3}, \alpha_1 = \alpha_2 = \frac{4\eta m_o}{\nu bh^3}, a = \frac{\sqrt{2}\eta}{\nu b}(h - m_o), \tag{3}$$

where H, b, G, and ν represent the tension density, cross-sectional area, Young's modulus, and the mass density of each strand, h is the distance between the strands, while η is the stiffness and m_o is the membrane height in positive equilibrium. The difference between the longitudinal displacements of the bottom and top strands is u in equation (1), as opposed to v, which represents the difference between the transverse displacements of the lower and higher strands.

Noq using a transformation:

$$v = eu + f, \tag{4}$$

where e and f are constants, to simplify Equation (1) into the system of equations as follows:

$$u_{\tau\tau} - \beta_1^2 u_{xx} = u^3(\eta_1 + \alpha_1 e^2) + u^2(2\alpha_1 ef + \xi_1 e) + u(\sigma_1 + f\xi_1 + \alpha_1 f^2), \tag{5}$$

$$u_{\tau\tau} - \beta_2^2 u_{xx} = u^3(\eta_2 + \alpha_2 e^2) + u^2\left(3\alpha_2 ef + \frac{\xi_2}{e} + \frac{\eta_2 f}{e}\right) + u\left(\sigma_2 + 3\alpha_2 f^2\right) + \frac{\sigma_2 f}{e} + \frac{\alpha_2 f^3}{e} + \frac{a}{e}. \tag{6}$$

Comparing Equations (4) and (5), we infer that $f = h/\sqrt{2}$ and $H = G$. So, Equation (5) can be written as

$$u_{\tau\tau} - \beta_1^2 u_{xx} = Su^3 + Tu^2 + Vu, \tag{7}$$

where

$$S = \frac{\zeta}{h^3}\left(-2 + 4e^2\right), \quad T = \frac{6\sqrt{2}e\zeta}{h^2}, \quad V = \left(\frac{-2\zeta}{m_o} + \frac{6\zeta}{h}\right), \quad \zeta = \frac{\eta m_o}{\nu b}, \quad \beta_1 = \frac{G}{\nu}. \tag{8}$$

3. Mathematical Analysis

The wave transformation $u(x, \tau) = u(\delta), \delta = lx + \kappa\tau$ reduces Equation (7) to the following ODE:

$$\left(\kappa^2 - l^2\beta_1^2\right)u'' - Su^3 - Tu^2 - Vu = 0, \text{where } \kappa^2 - l^2\beta_1^2 \neq 0. \tag{9}$$

According to [50, 51], a fractal DNA model can be written as

$$\left(\kappa^2 - l^2\beta_1^2\right)\frac{d}{d\delta^\gamma}\left(\frac{du}{d\delta^\gamma}\right) - Su^3 - Tu^2 - Vu = 0, \tag{10}$$

where γ and $du/d\delta^\gamma$ are the fractal dimensional value and derivative, respectively, stated as

$$\frac{du}{d\delta^\gamma} = \Gamma(1+\kappa)\lim_{\delta-\delta_o\longrightarrow\Delta\delta}\frac{u(\delta)-u(\delta_o)}{(\delta-\delta_o)^\kappa}, \quad \Delta\delta \neq 0. \tag{11}$$

The variational principle [44] can be used to produce the following trial-functional:

$$J = \int L d\delta = \int (K - E) d\delta. \tag{12}$$

The variational formulation of Equation (10) is given as

$$J = \int_0^\infty \left[\left(\kappa^2 - l^2\beta_1^2\right)\left(\frac{du}{d\delta^\gamma}\right)^2 + Su^3 + Tu^2 + Vu\right] d\delta^\gamma, \tag{13}$$

where $K = (\kappa^2 - l^2\beta_1^2)[du/d\delta^\gamma]^2$ is the kinetic energy and $E = -Su^3 - Tu^2 - Vu$ is the potential energy.

$$\begin{aligned} L &= \left(\kappa^2 - l^2\beta_1^2\right)\left(\frac{du}{d\delta^\gamma}\right)^2 + Su^3 + Tu^2 + Vu, \\ H &= \left(\kappa^2 - l^2\beta_1^2\right)\left(\frac{du}{d\delta^\gamma}\right)^2 - Su^3 - Tu^2 - Vu. \end{aligned} \tag{14}$$

The above equations are the Lagrangian and Hamiltonian. Using the two scale transformation,

$$A = \delta^\gamma. \tag{15}$$

Equation. (13) can be written as

$$J = \int_0^\infty \left[\left(\kappa^2 - l^2\beta_1^2\right)\left(\frac{du}{dA}\right)^2 + Su^3 + Tu^2 + Vu\right] dA. \tag{16}$$

3.1. Soliton Solutions of Fractal Model. Using Ritz technique, one can construct the solitary wave solution as

$$u = C\,\mathrm{sec}\,h(DA), \tag{17}$$

where C and D are constants to be further calculated. Putting Equation (17) into Equation (16), we have

$$J = \frac{C^2}{12D}\left(\pi CT + 6V + 2SC^2\right) + \frac{C^2 D}{6}\left(\kappa^2 - l^2\beta_1^2\right). \tag{18}$$

Setting J stationary with respect to C and D, it results,

$$\frac{\partial J}{\partial C} = \frac{C}{12D}\left(3\pi CT + 12V + 8SC^2\right) + \frac{CD}{3}\left(\kappa^2 - l^2\beta_1^2\right), \tag{19}$$

$$\frac{\partial J}{\partial D} = -\frac{C^2}{12D^2}\left(\pi CT + 6V + 2SC^2\right) + \frac{C^2}{6}\left(\kappa^2 - l^2\beta_1^2\right). \tag{20}$$

From Equations (19) and (20), we have

$$\begin{aligned} C &= \pm\frac{\left(-5\pi T + \sqrt{25\pi^2T^2 - 1152SV}\right)}{24S}, \\ D &= \pm\sqrt{\frac{\left(5\pi T - \sqrt{25\pi^2T^2 - 1152SV}\right)\pi T - 288SV}{288\left(l^2\beta_1^2 - \kappa^2\right)S}}. \end{aligned} \tag{21}$$

Now, Equation (17) can be described as

$$\begin{aligned} u(x,\tau) = {} & \pm\frac{\left(-5\pi T + \sqrt{25\pi^2T^2 - 1152SV}\right)}{24S} \\ & \mathrm{sec}\,h\left[\pm\sqrt{\frac{\left(5\pi T - \sqrt{25\pi^2T^2 - 1152SV}\right)\pi T - 288SV}{288\left(l^2\beta_1^2 - \kappa^2\right)S}}A\right]. \end{aligned} \tag{22}$$

Inserting the value of u in Equation (4), then, we have

$$\begin{aligned} v(x,\tau) = {} & \pm e\frac{\left(-5\pi T + \sqrt{25\pi^2T^2 - 1152SV}\right)}{24S} \\ & \mathrm{sec}\,h\left[\pm\sqrt{\frac{\left(5\pi T - \sqrt{25\pi^2T^2 - 1152SV}\right)\pi T - 288SV}{288\left(l^2\beta_1^2 - \kappa^2\right)S}}A\right] + f, \end{aligned} \tag{23}$$

where $A = (lx + \kappa\tau)^\gamma$.

Additionally, we look another soliton solution in the form:

$$u = P\,\mathrm{sec}\,h^4(QA), \tag{24}$$

where P and Q are constants to be further calculated. Substituting Equation (24) in Equation (16), we have

$$J = \frac{P^2}{135135Q}\left(16640PT + 30888V + 10752SP^2\right) + \frac{128P^2Q}{315}\left(\kappa^2 - l^2\beta_1^2\right). \tag{25}$$

When we keep J stationary with respect to P and Q, it gives

$$\frac{\partial J}{\partial P} = \frac{P}{45045Q}\left(16640PT + 20592V + 14336SP^2\right) + \frac{256PQ}{315}\left(\kappa^2 - l^2\beta_1^2\right), \tag{26}$$

$$\frac{\partial J}{\partial Q} = -\frac{P^2}{135135Q^2}\left(16640PT + 30888V + 10752SP^2\right) + \frac{128P^2}{315}\left(\kappa^2 - l^2\beta_1^2\right). \tag{27}$$

From Equations (26) and (27), we have

$$P = \pm \frac{\left(-325T + \sqrt{105625T^2 - 486486SV}\right)}{504S},$$
$$Q = \pm \sqrt{\frac{10T\left(325T - \sqrt{105625T^2 - 486486SV}\right) - 18711SV}{99792\left(l^2\beta_1^2 - \kappa^2\right)S}}. \tag{28}$$

Equation (24) becomes

$$u(x,\tau) = \pm \frac{\left(-325T + \sqrt{105625T^2 - 486486SV}\right)}{504S} \sec h^4\left[\pm \sqrt{\frac{10T\left(325T - \sqrt{105625T^2 - 486486SV}\right) - 18711SV}{99792\left(l^2\beta_1^2 - \kappa^2\right)S}} A\right]. \tag{29}$$

Plugging the value of u in Equation (4), we have

$$v(x,\tau) = \pm e^{\frac{\left(-325T + \sqrt{105625T^2 - 486486SV}\right)}{504S}} \sec h^4\left[\pm \sqrt{\frac{10T\left(325T - \sqrt{105625T^2 - 486486SV}\right) - 18711SV}{99792\left(l^2\beta_1^2 - \kappa^2\right)S}} A\right] + f \tag{30}$$

where $A = (lx + \kappa\tau)^{\gamma}$.

4. Illustration of the AEM

The following statement illustrates the general NLPDE structure:

$$Q(u, u_t, u_x, uu_t, u_t u_{xx}, uu_{tt}, \cdots) = 0, \tag{31}$$

where Q is polynomial function of u and its derivatives in relation to two independent variables t and x. Use the single variable conversion $\delta = lx - \kappa t$ to reduce Equation (31) into ODE of the form:

$$R\left(u, u', u'', uu'', \cdots\right) = 0. \tag{32}$$

Here, R is a polynomial function with both linear and nonlinear terms and the superscripts of u show its ordinary derivative with respect to δ. The algorithm of AEM suggests the initial solution of Equation (32) as

$$u(\delta) = \sum_{i=0}^{M} d_i \beta^{i\phi(\delta)}, \tag{33}$$

satisfying the auxiliary equation

$$\phi'(\delta) = \frac{1}{\ln(\beta)}\left(a\beta^{-\phi(\delta)} + c + b\beta^{\phi(\delta)}\right), \tag{34}$$

where $d_0, d_1, d_2, \ldots, d_M$ are coefficients to be evaluated such that $d_M \neq 0$. The value of M is determined by balancing the highest order derivative and nonlinear term involved in Equation (9).

Now, putting Equation (33) into Equation (9) and performing few steps of algebra yields a system of algebraic equations in $\beta^{\phi(\delta)}$.

The family of solutions of Equation (34) can be obtained as follows:

Family 1. When $c^2 - 4ab < 0$ and $b \neq 0$,

$$\beta^{\phi(\delta)} = \frac{-c}{2b} + \frac{\sqrt{4ab - c^2}}{2b} \tan\left(\frac{\sqrt{4ab - c^2}}{2}\delta\right),$$
$$\beta^{\phi(\delta)} = \frac{-c}{2b} - \frac{\sqrt{4ab - c^2}}{2b} \cot\left(\frac{\sqrt{4ab - c^2}}{2}\delta\right). \tag{35}$$

Family 2. When $c^2 - 4ab > 0$ and $b \neq 0$,

$$\beta^{\phi(\delta)} = \frac{-c}{2b} - \frac{\sqrt{c^2 - 4ab}}{2b} \tan h\left(\frac{\sqrt{c^2 - 4ab}}{2}\delta\right),$$
$$\beta^{\phi(\delta)} = \frac{-c}{2b} - \frac{\sqrt{c^2 - 4ab}}{2b} \cot h\left(\frac{\sqrt{c^2 - 4ab}}{2}\delta\right). \tag{36}$$

Family 3. When $c^2 + 4a^2 < 0$ and $b \neq 0$ and $b = -a$,

$$\beta^{\phi(\delta)} = \frac{c}{2a} - \frac{\sqrt{-4a^2 - c^2}}{2a} \tan\left(\frac{\sqrt{-4a^2 - c^2}}{2}\delta\right),$$
$$\beta^{\phi(\delta)} = \frac{c}{2a} + \frac{\sqrt{-4a^2 - c^2}}{2a} \cot\left(\frac{\sqrt{-4a^2 - c^2}}{2}\delta\right). \tag{37}$$

Family 4. When $c^2 + 4a^2 < 0$ and $b \neq 0$ and $b = -a$,

$$\beta^{\phi(\delta)} = \frac{c}{2a} + \frac{\sqrt{4a^2 + c^2}}{2a} \tan h\left(\frac{\sqrt{4a^2 + c^2}}{2}\delta\right),$$
$$\beta^{\phi(\delta)} = \frac{c}{2a} + \frac{\sqrt{4a^2 + c^2}}{2a} \cot h\left(\frac{\sqrt{4a^2 + c^2}}{2}\delta\right). \tag{38}$$

Family 5. When $c^2 - 4a^2 < 0$ and $b = a$,

$$\beta^{\phi(\delta)} = \frac{-c}{2a} + \frac{\sqrt{4a^2 - c^2}}{2a} \tan\left(\frac{\sqrt{4a^2 - c^2}}{2}\delta\right),$$
$$\beta^{\phi(\delta)} = \frac{-c}{2a} - \frac{\sqrt{4a^2 - c^2}}{2a} \cot\left(\frac{\sqrt{4a^2 - c^2}}{2}\delta\right). \tag{39}$$

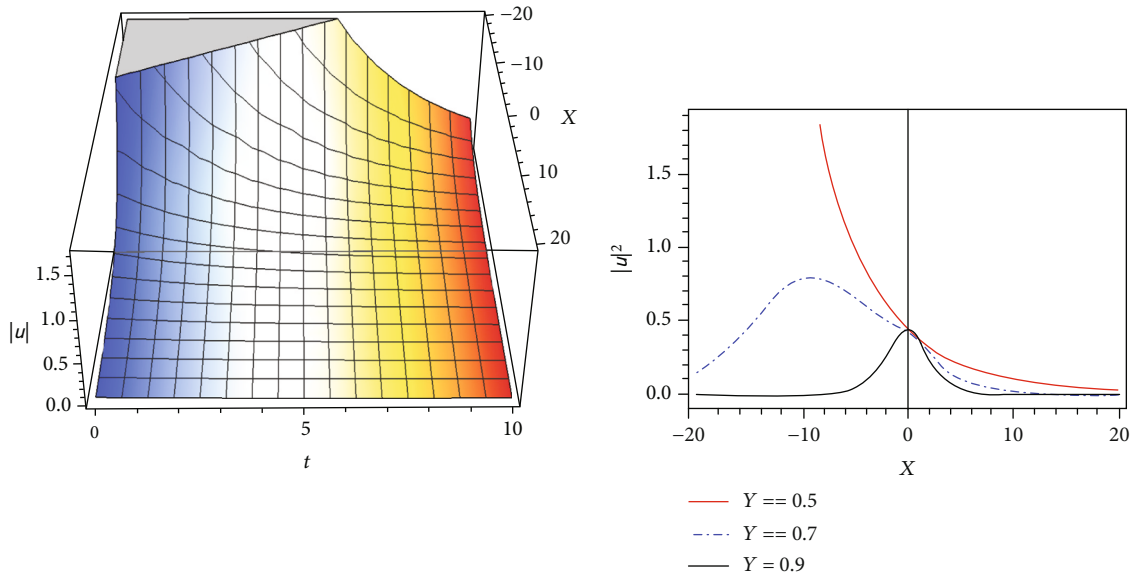

(a) (b)

FIGURE 1: We consider $\kappa = 2$, $l = 1$, $\beta_1 = 1$, $S = -1$, $T = 2$, $V = 1$, and $\gamma = 0.5,0.7,0.9$ for the solution described by Equation (22). (a) The 3D sketch of $|u|^2$ taking $\gamma = 0.5$. (b) 2D-plot of $|u|^2$ with three distinct γ values.

Family 6. When $c^2 - 4a^2 > 0$ and $b = a$,

$$\beta^{\phi(\delta)} = \frac{-c}{2a} - \frac{\sqrt{-4a^2 + c^2}}{2a} \tan h\frac{\sqrt{-4a^2 + c^2}}{2}\delta\Big),$$
$$\beta^{\phi(\delta)} = \frac{-c}{2a} - \frac{\sqrt{-4a^2 + c^2}}{2a} \cot h\left(\frac{\sqrt{-4a^2 + c^2}}{2}\delta\right). \tag{40}$$

Family 7. When $c^2 = 4ab$,

$$\beta^{\phi(\delta)} = -\frac{2 + c\delta}{2b\delta}. \tag{41}$$

Family 8. When $ab < 0$, $c = 0$ and $b \neq 0$,

$$\beta^{\phi(\delta)} = -\sqrt{\frac{-a}{b}} \tan h\left(\sqrt{-ba}\delta\right),$$
$$\beta^{\phi(\delta)} = -\sqrt{\frac{-a}{b}} \cot h\left(\sqrt{-ba}\delta\right). \tag{42}$$

Family 9. When $c = 0$ and $a = -b$,

$$\beta^{\phi(\delta)} = \frac{1 + e^{-2b\delta}}{-1 + e^{-2b\delta}}. \tag{43}$$

Family 10. When $a = b = 0$,

$$\beta^{\phi(\delta)} = \cos h(c\delta) + \sin h(c\delta). \tag{44}$$

Family 11. When $a = c = K$ and $b = 0$,

$$\beta^{\phi(\delta)} = e^{K\delta} - 1. \tag{45}$$

Family 12. When $b = c = K$ and $a = 0$,

$$\beta^{\phi(\delta)} = \frac{e^{K\delta}}{1 - e^{K\delta}}. \tag{46}$$

Family 13. When $c = a + b$,

$$\beta^{\phi(\delta)} = -\frac{1 - ae^{(a-b)\delta}}{1 - be^{(a-b)\delta}}. \tag{47}$$

Family 14. When $c = -(a + b)$,

$$\beta^{\phi(\delta)} = \frac{a - e^{(a-b)\delta}}{b - e^{(a-b)\delta}}. \tag{48}$$

Family 15. When $a = 0$,

$$\beta^{\phi(\delta)} = \frac{ce^{c\delta}}{1 - be^{c\delta}}. \tag{49}$$

Family 16. When $c = a = b \neq 0$,

$$\beta^{\phi(\delta)} = \frac{1}{2}\left[\sqrt{3} \tan\left(\frac{\sqrt{3}}{2}a\delta\right) - 1\right]. \tag{50}$$

Family 17. When $a = b$ and $c = 0$,

$$\beta^{\phi(\delta)} = \tan(a\delta). \tag{51}$$

Family 18. When $b = 0$,

$$\beta^{\phi(\delta)} = e^{c\delta} - \frac{m}{n}. \tag{52}$$

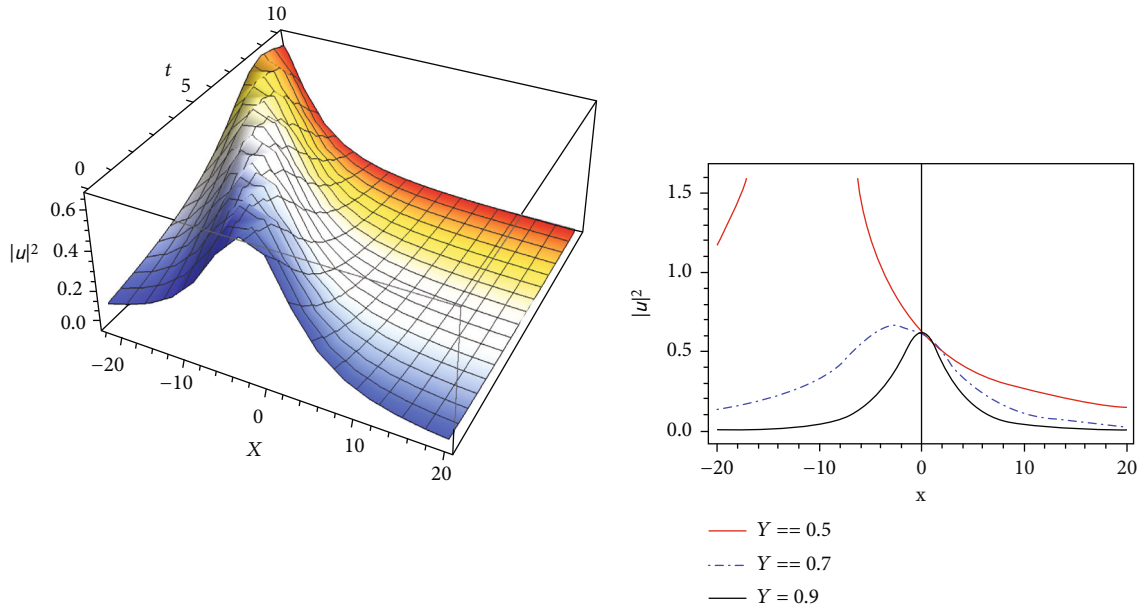

(a) (b)

FIGURE 2: We suggest $\kappa = 2$, $l = 1$, $\beta_1 = 1$, $S = -1$, $T = 2$, $V = 1$, and $\gamma = 0.5,0.7,0.9$ for the solution obtained in Equation (29). (a) The 3D-plot of $|u|^2$ with $\gamma = 0.7$. (b) The 2D-plot of $|u|^2$ with distinct values of γ.

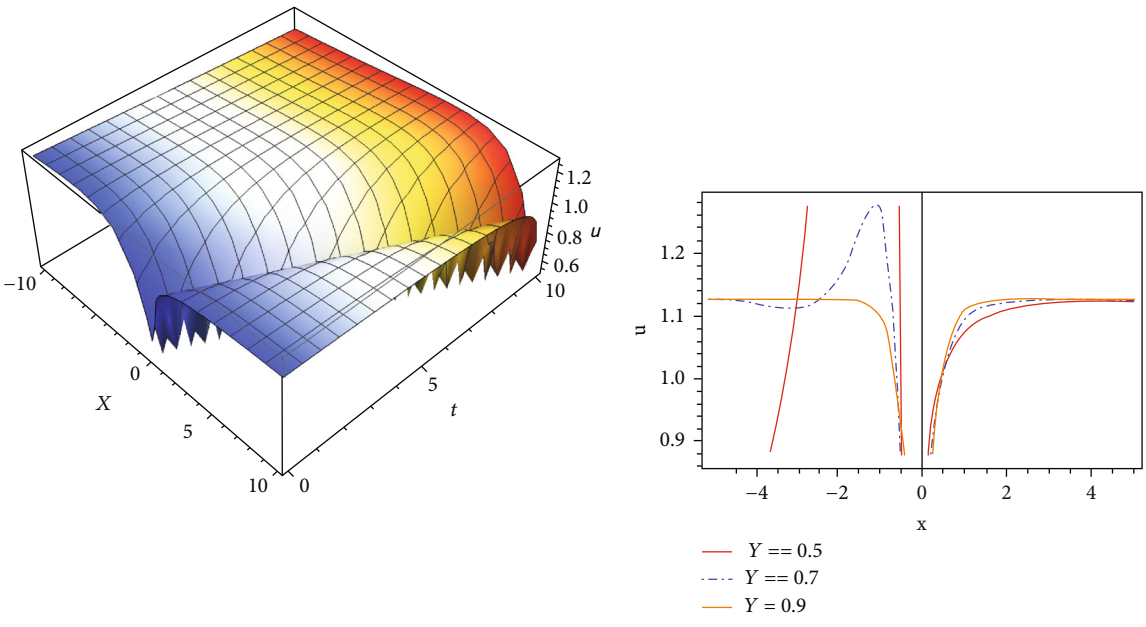

(a) (b)

FIGURE 3: We suggest $\kappa = -1$, $\beta_1 = 1$, $T = 2$, $V = 1$, $c = 3$, $a = 1$, $b = 1$, and $\gamma = 0.5,0.7,0.9$. for the solution $u_{1,1}$. (a) The 3D graph of $u_{1,1}(x,t)$ with $\gamma = 0.3$. (b) The 2D graph of $u_{1,1}(x,t)$ with distinct values of γ.

4.1. Application of AEM. The balancing principle employed to Equation (9) yields the value of index $M = 1$. Hence, Equation (33) takes the form:

$$u(\delta) = d_0 + d_1\beta^{\phi(\delta)}. \tag{53}$$

Now, invoking Equation (53) into Equation (9) gives a system of equations which is further evaluated via Maple, it generates

$$\begin{aligned} d_0 &= \frac{3V(q\Theta - 1)}{2T}, d_1 = \frac{3bV\Theta}{T}, S = \frac{2T^2}{9V}, l \\ &= \frac{-\sqrt{(4ab\kappa^2 - c^2\kappa^2)/\Theta} - V}{\beta_1}, \end{aligned} \tag{54}$$

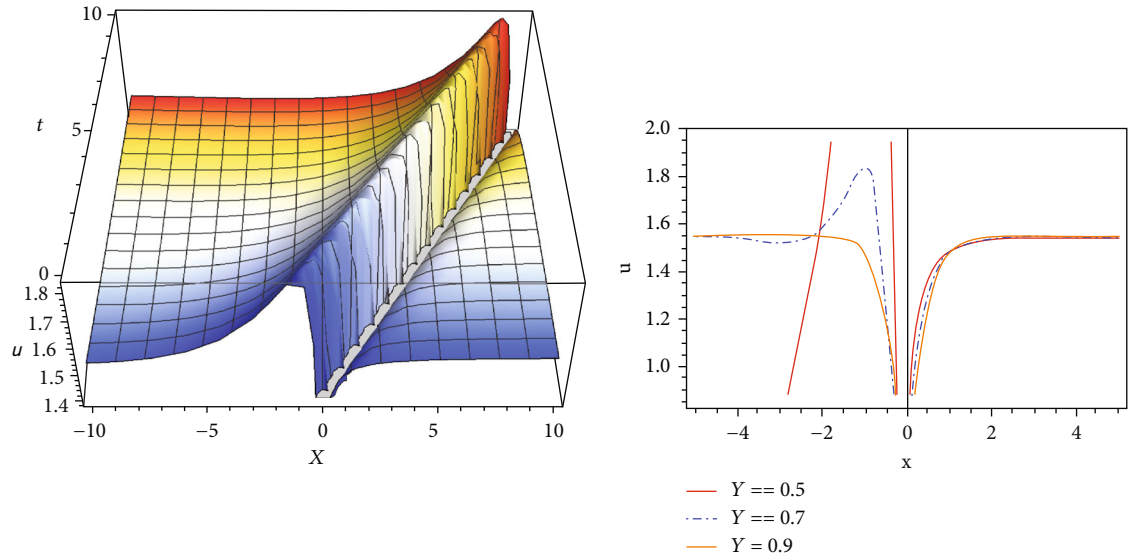

(a) (b)

FIGURE 4: We take $\kappa = -1$, $\beta_1 = 1$, $T = 2$, $V = 1$, $c = 3$, $a = 1$, $b = 1$, and $\gamma = 0.5,0.7,0.9$. for the solution $|u_{3,1}|$. (a) The 3D graph of $u_{3,1}(x,t)$ with $\gamma = 0.3$. (b) The 2D graph of $u_{3,1}(x,t)$ with distinct values of γ.

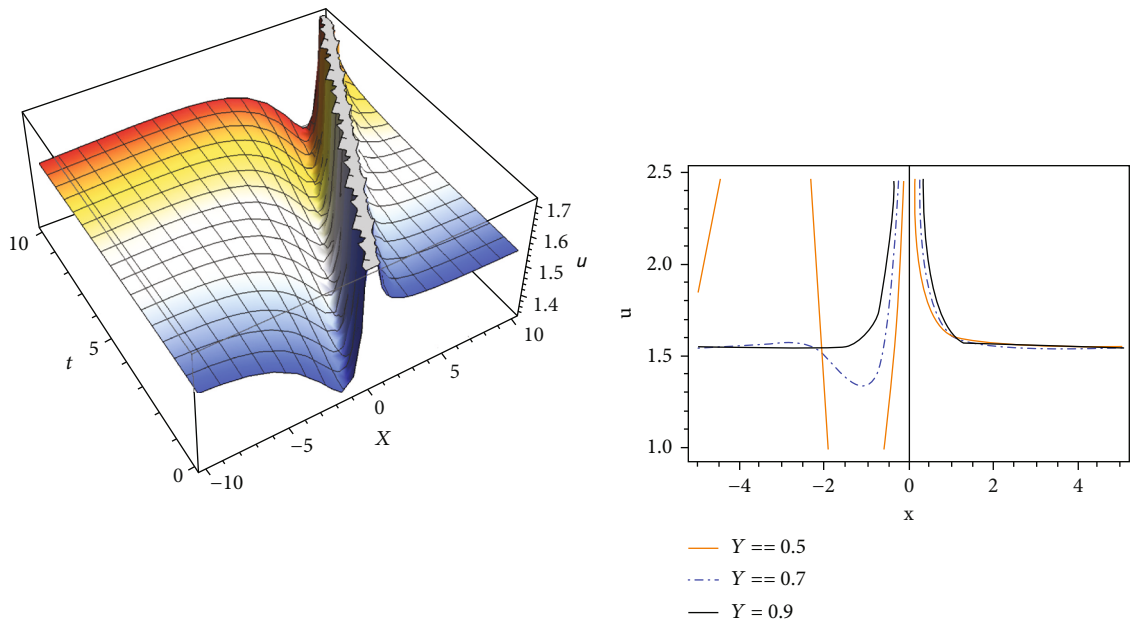

(a) (b)

FIGURE 5: We take $\kappa = -1$, $\beta_1 = 1$, $T = 2$, $V = 1$, $c = 3$, $a = 1$, $b = 1$, and $\gamma = 0.5,0.7,0.9$ for the solution $|u_{3,2}|$. (a) The 3D graph of $u_{3,2}(x,t)$ with $\gamma = 0.3$. (b) The 2D graph of $u_{3,2}(x,t)$ with distinct values of γ.

where

$$\Theta = \sqrt{\frac{-1}{4ab - c^2}}. \tag{55}$$

Insertion of Equation (54) into Equation (53) results to

$$u(\delta) = \frac{3V(c\Theta - 1)}{2T} + \frac{3bV\Theta}{T}\beta^{\phi(\delta)}. \tag{56}$$

By substituting the solutions specified by Equation (34) into Equation (58), the solutions retrieved are

For Family 1, when $c^2 - 4ab < 0$ and $b \neq 0$,

$$u_{1,1}(x,t) = \frac{3V(c\Theta - 1)}{2T} + \frac{3V\Theta}{T}\left[\frac{-c}{2} + \sqrt{4ab - c^2}\tan\left(\frac{\sqrt{4ab - c^2}}{2}\delta^{\gamma}\right)\right], \tag{57}$$

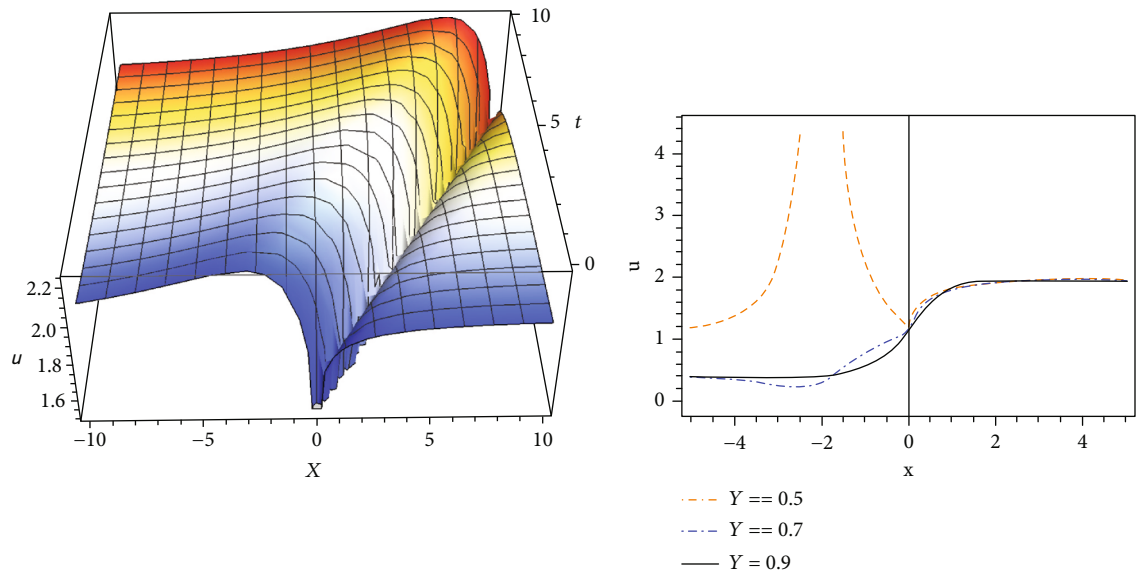

(a) (b)

FIGURE 6: We take $\kappa = -1$, $\beta_1 = 1$, $T = 2$, $V = 1$, $c = 3$, $a = 1$, $b = 1$, and $\gamma = 0.5,0.7,0.9$ for the solution $|u_{5,1}|$. (a) The 3D graph of $u_{5,1}(x,t)$ with $\gamma = 0.3$. (b) The 2D graph of $u_{5,1}(x,t)$ with distinct values of γ.

$$u_{1,2}(x,t) = \frac{3V(c\Theta-1)}{2T} + \frac{3V\Theta}{T}\left[\frac{-c}{2} - \sqrt{4ab-c^2}\cot\left(\frac{\sqrt{4ab-c^2}}{2}\delta^{\gamma}\right)\right], \tag{58}$$

$$v_{1,1}(x,t) = \frac{3eV(c\Theta-1)}{2T} + \frac{3eV\Theta}{T}\left[\frac{-c}{2} + \sqrt{4ab-c^2}\tan\left(\frac{\sqrt{4ab-c^2}}{2}\delta^{\gamma}\right)\right] + f, \tag{59}$$

$$v_{1,2}(x,t) = \frac{3eV(c\Theta-1)}{2T} + \frac{3eV\Theta}{T}\left[\frac{-c}{2} - \sqrt{4ab-c^2}\cot\left(\frac{\sqrt{4ab-c^2}}{2}\delta^{\gamma}\right)\right] + f. \tag{60}$$

For Family 2, when $c^2 - 4ab > 0$ and $b \neq 0$,

$$u_{2,1}(x,t) = \frac{3V(c\Theta-1)}{2T} + \frac{3V\Theta}{T}\left[\frac{-c}{2} - \sqrt{c^2-4ab}\tan h\left(\frac{\sqrt{c^2-4ab}}{2}\delta^{\gamma}\right)\right],$$

$$u_{2,2}(x,t) = \frac{3V(c\Theta-1)}{2T} + \frac{3V\Theta}{T}\left[\frac{-c}{2} - \sqrt{c^2-4ab}\cot h\left(\frac{\sqrt{c^2-4ab}}{2}\delta^{\gamma}\right)\right],$$

$$v_{2,1}(x,t) = \frac{3eV(c\Theta-1)}{2T} + \frac{3eV\Theta}{T}\left[\frac{-c}{2} - \sqrt{c^2-4ab}\tan h\left(\frac{\sqrt{c^2-4ab}}{2}\delta^{\gamma}\right)\right] + f,$$

$$v_{2,2}(x,t) = \frac{3eV(c\Theta-1)}{2T} + \frac{3eV\Theta}{T}\left[\frac{-c}{2} - \sqrt{c^2-4ab}\cot h\left(\frac{\sqrt{c^2-4ab}}{2}\delta^{\gamma}\right)\right] + f. \tag{61}$$

For Family 3, when $c^2 + 4ab < 0$, $b \neq 0$ and $b = -a$,

$$u_{3,1}(x,t) = \frac{3V(c\Theta-1)}{2T} - \frac{3V\Theta}{T}\left[\frac{c}{2} - \sqrt{4a^2-c^2}\tan\left(\frac{\sqrt{4a^2-c^2}}{2}\delta^{\gamma}\right)\right],$$

$$u_{3,2}(x,t) = \frac{3V(c\Theta-1)}{2T} - \frac{3V\Theta}{T}\left[\frac{c}{2} + \sqrt{4a^2-c^2}\cot\left(\frac{\sqrt{4a^2-c^2}}{2}\delta^{\gamma}\right)\right],$$

$$v_{3,1}(x,t) = \frac{3eV(c\Theta-1)}{2T} - \frac{3eV\Theta}{T}\left[\frac{c}{2} - \sqrt{4a^2-c^2}\tan\left(\frac{\sqrt{4a^2-c^2}}{2}\delta^{\gamma}\right)\right] + f,$$

$$v_{3,2}(x,t) = \frac{3eV(c\Theta-1)}{2T} - \frac{3eV\Theta}{T}\left[\frac{c}{2} + \sqrt{4a^2-c^2}\cot\left(\frac{\sqrt{4a^2-c^2}}{2}\delta^{\gamma}\right)\right] + f. \tag{62}$$

For Family 4, when $c^2 + 4a^2 > 0$, $b \neq 0$ and $b = -a$,

$$u_{4,1}(x,t) = \frac{3V(c\Theta-1)}{2T} - \frac{3V\Theta}{T}\left[\frac{c}{2} + \sqrt{4a^2+c^2}\tan h\left(\frac{\sqrt{4a^2+c^2}}{2}\delta^{\gamma}\right)\right],$$

$$u_{4,2}(x,t) = \frac{3V(c\Theta-1)}{2T} - \frac{3V\Theta}{T}\left[\frac{c}{2} + \sqrt{4a^2+c^2}\cot h\left(\frac{\sqrt{4a^2+c^2}}{2}\delta^{\gamma}\right)\right],$$

$$v_{4,1}(x,t) = \frac{3eV(c\Theta-1)}{2T} - \frac{3eV\Theta}{T}\left[\frac{c}{2} + \sqrt{4a^2+c^2}\tan h\left(\frac{\sqrt{4a^2+c^2}}{2}\delta^{\gamma}\right)\right] + f,$$

$$v_{4,2}(x,t) = \frac{3eV(c\Theta-1)}{2T} - \frac{3eV\Theta}{T}\left[\frac{c}{2} + \sqrt{4a^2+c^2}\cot h\left(\frac{\sqrt{4a^2+c^2}}{2}\delta^{\gamma}\right)\right] + f. \tag{63}$$

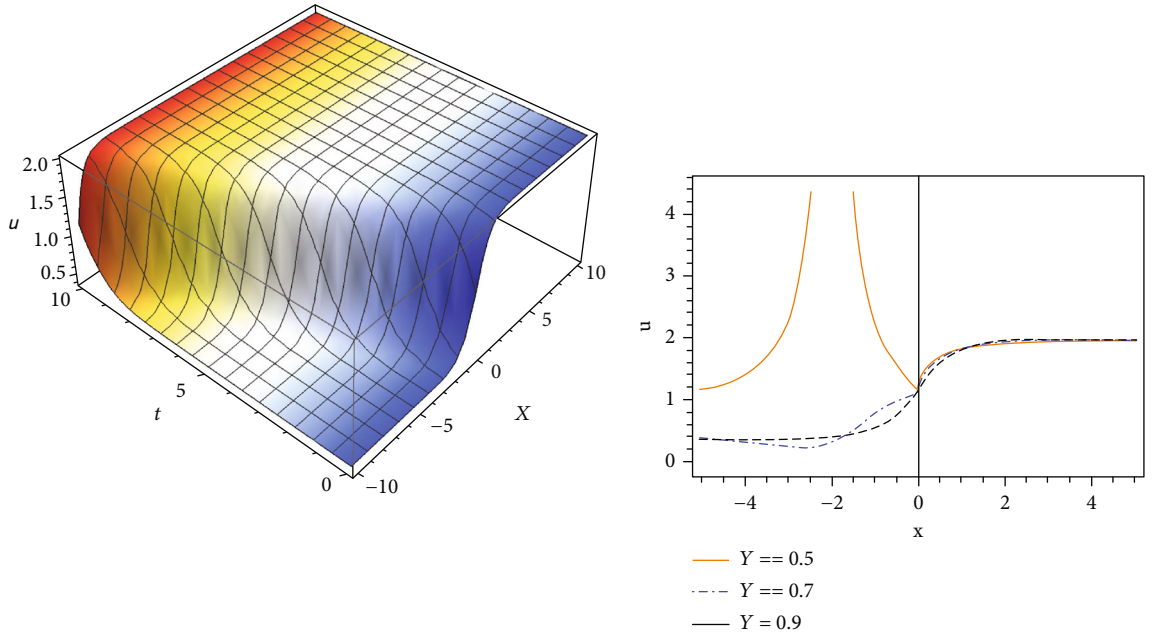

(a) (b)

FIGURE 7: We consider $\kappa = -1$, $\beta_1 = 1$, $T = 2$, $V = 1$, $c = 3$, $a = 1$, $b = 1$, and $\gamma = 0.5,0.7,0.9$ for the solution $|u_{6,1}|$. (a) The 3D graph of $u_{6,1}(x, t)$ with $\gamma = 0.8$. (b) The 2D graph of $u_{6,1}(x, t)$ with distinct values of γ.

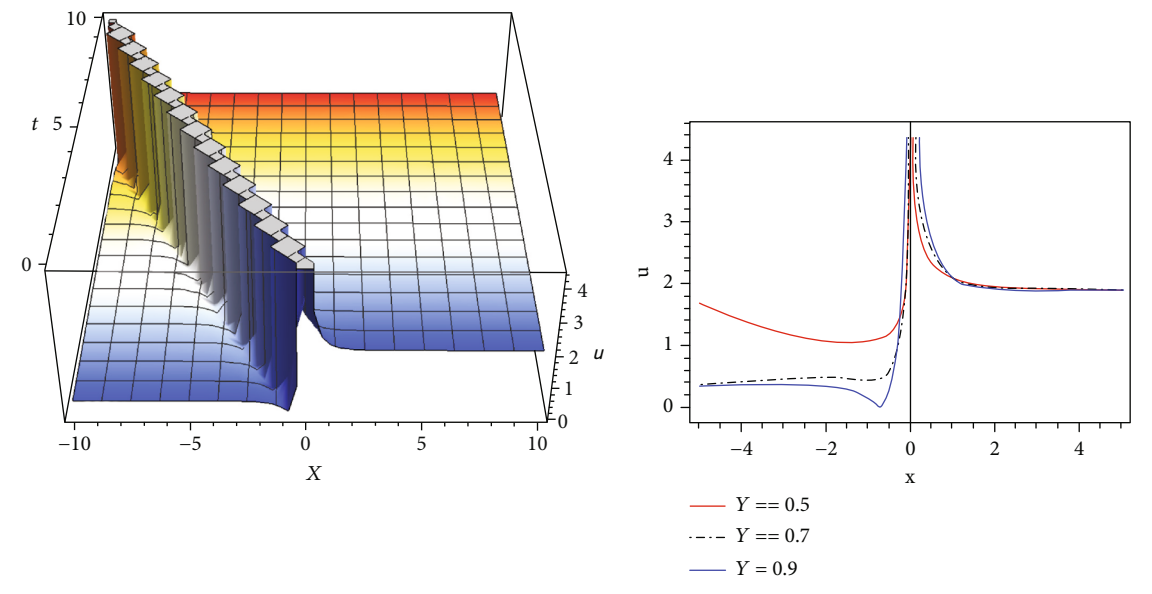

(a) (b)

FIGURE 8: We suggest $\kappa = -1$, $\beta_1 = 1$, $T = 2$, $V = 1$, $c = 3$, $a = 1$, $b = 1$, and $\gamma = 0.5,0.7,0.9$ for the solution $|u_{6,2}|$. (a) The 3D graph of $u_{6,2}(x, t)$ with $\gamma = 0.3$. (b) The 2D graph of $u_{6,2}(x, t)$ with distinct values of γ.

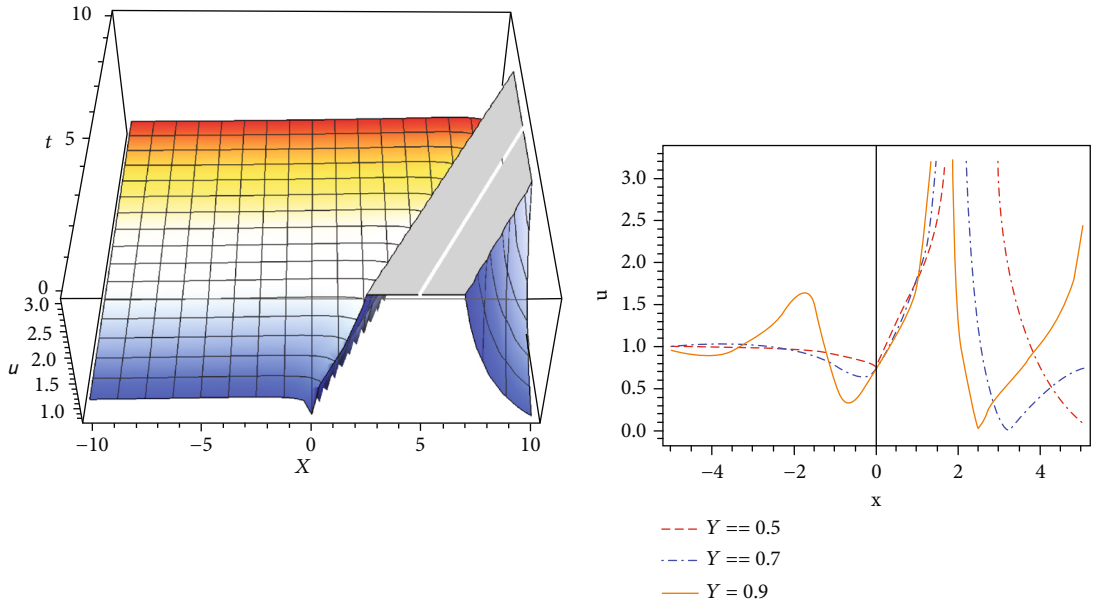

(a) (b)

FIGURE 9: We take $\kappa = -1$, $\beta_1 = 1$, $T = 2$, $V = 1$, $c = 3$, $a = 1$, $b = 1$, and $\gamma = 0.5,0.7,0.9$ for the solution $|u_{8,1}|$. (a) The 3D graph of $u_{8,1}(x,t)$ with $\gamma = 0.3$. (b) The 2D graph of $u_{8,1}(x,t)$ with distinct values of γ.

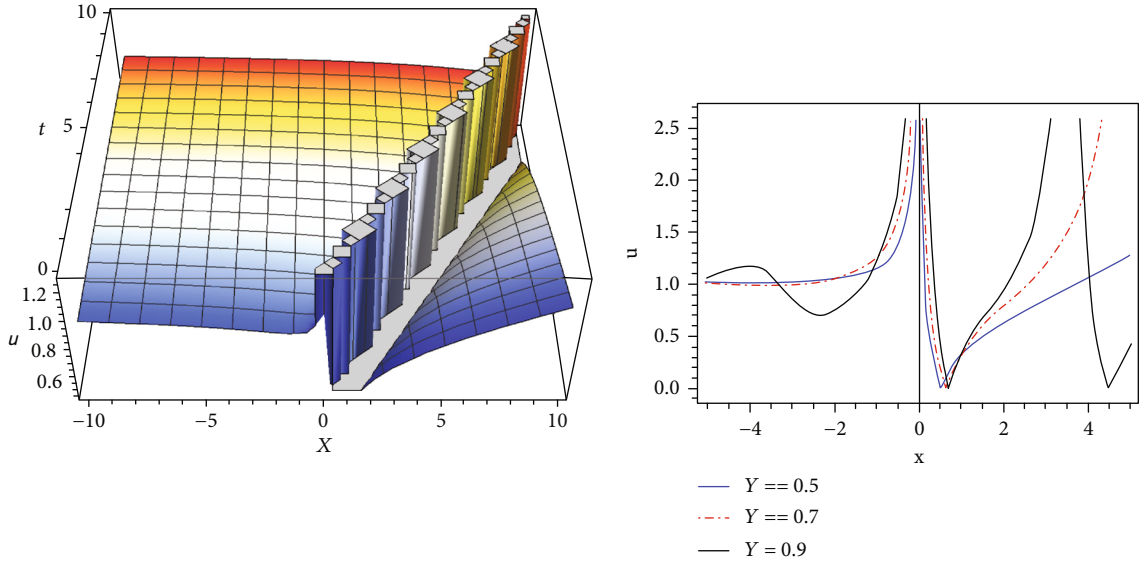

(a) (b)

FIGURE 10: We take $\kappa = -1$, $\beta_1 = 1$, $T = 2$, $V = 1$, $c = 3$, $a = 1$, $b = 1$, and $\gamma = 0.5,0.7,0.9$ for the solution $|u_{8,2}|$. (a) The 3D graph of $u_{8,2}(x,t)$ with $\gamma = 0.3$. (b) The 2D graph of $u_{8,2}(x,t)$ with distinct values of γ.

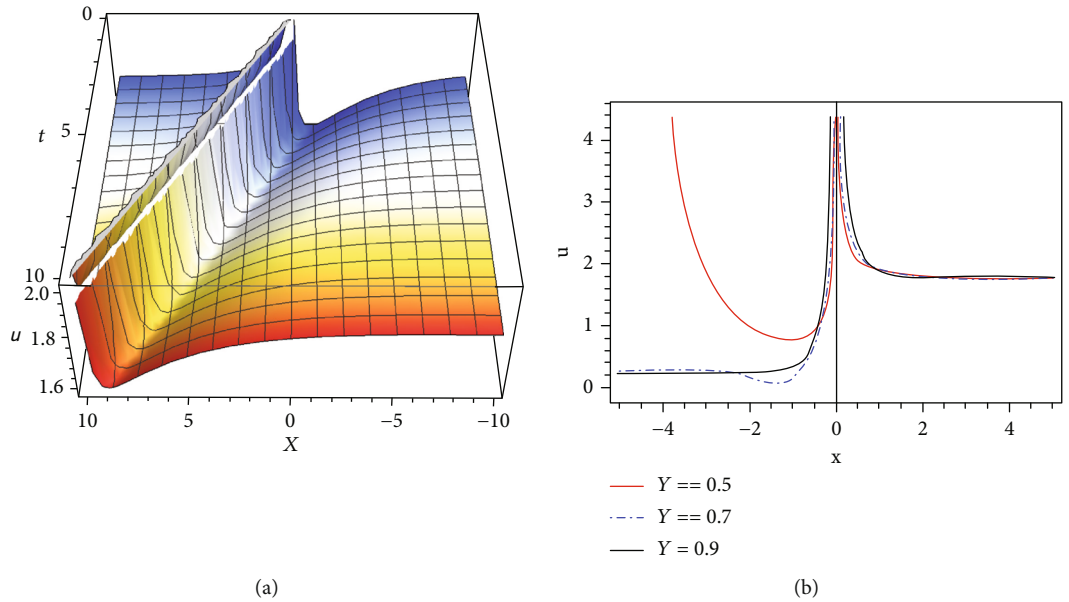

(a) (b)

FIGURE 11: In this figure, we take $\kappa = -1$, $\beta_1 = 1$, $T = 2$, $V = 1$, $c = 3$, $a = 1$, $b = 1$, and $\gamma = 0.5,0.7,0.9$ for the solution $|u_{15}|$. (a) The 3D graph of $u_{15}(x, t)$ with $\gamma = 0.3$. (b) The 2D graph of $u_{15}(x, t)$ with distinct values of γ.

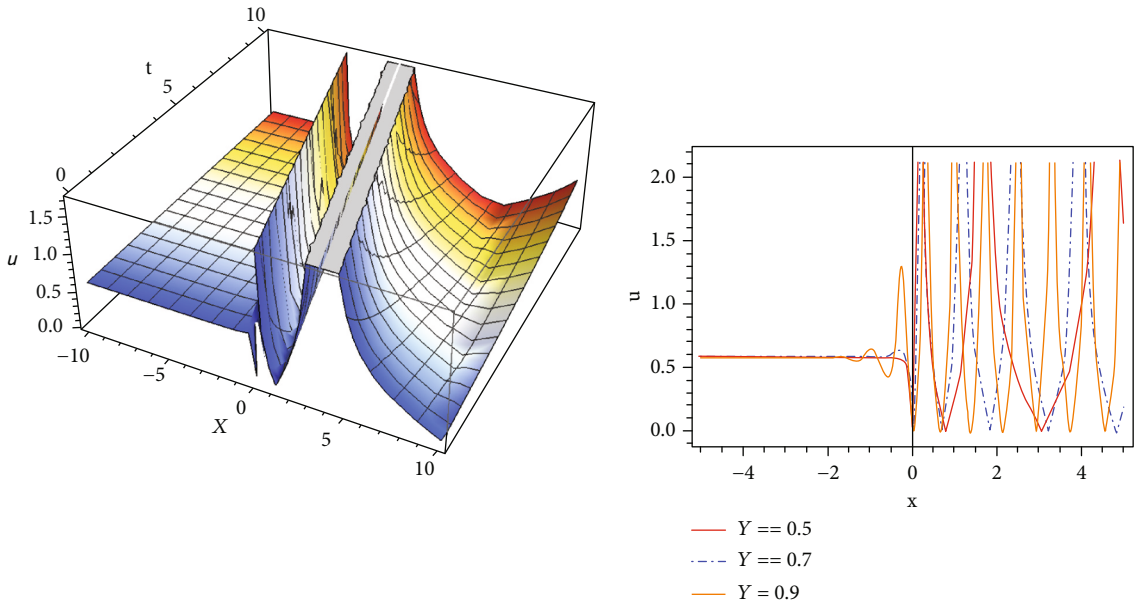

(a) (b)

FIGURE 12: In this figure, we take $\kappa = -1$, $\beta_1 = 1$, $T = 2$, $V = 1$, $c = 3$, $a = 1$, $b = 1$, and $\gamma = 0.5,0.7,0.9$ for the solution $|u_{16}|$. (a) The 3D graph of $u_{16}(x, t)$ with $\gamma = 0.3$. (b) The 2D graph of $u_{16}(x, t)$ with distinct values of γ.

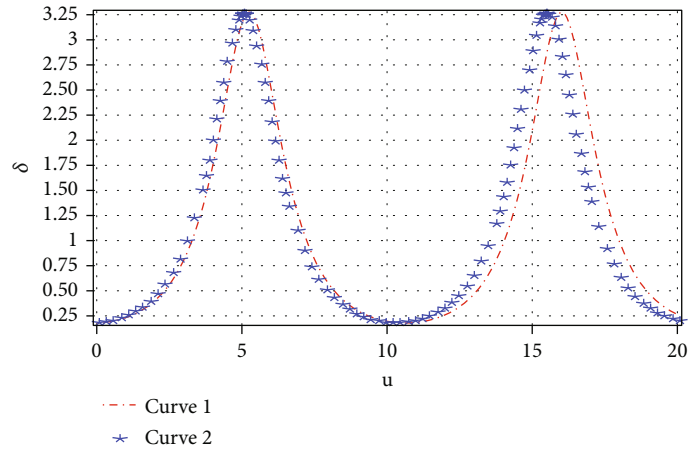

Figure 13: Sensitivity of model for initial conditions $(u, \delta) = (0.18,0.01)$ and $(u, \delta) = (0.2,0.02)$ with free parameters $S = -1$, $T = 2$, $V = 1$, $\kappa = 2$, $l = 1$, and $\beta_1 = 1$ while both conditions represent the curves in red and blue colors, respectively.

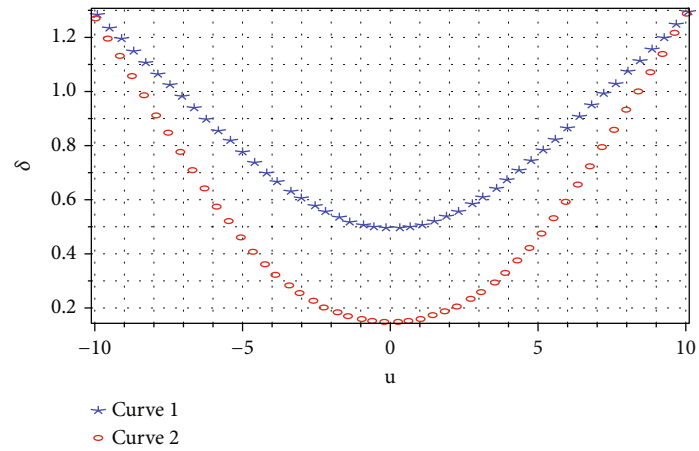

Figure 14: Sensitivity of model for initial conditions $(u, \delta) = (0.5,0.001)$ and $(u, \delta) = (0.15,0.001)$ with free parameters $S = 1$, $T = -2$, $V = 1$, $\kappa = 2$, $l = 1$, and $\beta_1 = 1$ while both conditions represent the curves in red and blue, respectively.

For Family 5, when $c^2 - 4a^2 < 0$ and $b = a$,

$$u_{5,1}(x,t) = \frac{3V(c\Theta - 1)}{2T} + \frac{3V\Theta}{T}\left[\frac{-c}{2} + \sqrt{4a^2 - c^2}\tan\left(\frac{\sqrt{4a^2 - c^2}}{2}\delta^{\gamma}\right)\right],$$

$$u_{5,2}(x,t) = \frac{3V(c\Theta - 1)}{2T} + \frac{3V\Theta}{T}\left[\frac{-c}{2} - \sqrt{4a^2 - c^2}\cot\left(\frac{\sqrt{4a^2 - c^2}}{2}\delta^{\gamma}\right)\right],$$

$$v_{5,1}(x,t) = \frac{3eV(c\Theta - 1)}{2T} + \frac{3eV\Theta}{T}\left[\frac{-c}{2} + \sqrt{4a^2 - c^2}\tan\left(\frac{\sqrt{4a^2 - c^2}}{2}\delta^{\gamma}\right)\right] + f,$$

$$v_{5,2}(x,t) = \frac{3eV(c\Theta - 1)}{2T} + \frac{3eV\Theta}{T}\left[\frac{-c}{2} - \sqrt{4a^2 - c^2}\cot\left(\frac{\sqrt{4a^2 - c^2}}{2}\delta^{\gamma}\right)\right] + f. \tag{64}$$

For Family 6, when $c^2 - 4a^2 > 0$ and $b = a$,

$$u_{6,1}(x,t) = \frac{3V(c\Theta - 1)}{2T} + \frac{3V\Theta}{T}\left[\frac{-c}{2} - \sqrt{-4a^2 + c^2}\tan h\left(\frac{\sqrt{-4a^2 + c^2}}{2}\delta^{\gamma}\right)\right],$$

$$u_{6,2}(x,t) = \frac{3V(c\Theta - 1)}{2T} + \frac{3V\Theta}{T}\left[\frac{-c}{2} - \sqrt{-4a^2 + c^2}\cot h\left(\frac{\sqrt{-4a^2 + c^2}}{2}\delta^{\gamma}\right)\right],$$

$$v_{6,1}(x,t) = \frac{3eV(c\Theta - 1)}{2T} + \frac{3eV\Theta}{T}\left[\frac{-c}{2} - \sqrt{-4a^2 + c^2}\tan h\left(\frac{\sqrt{-4a^2 + c^2}}{2}\delta^{\gamma}\right)\right] + f,$$

$$v_{6,2}(x,t) = \frac{3eV(c\Theta - 1)}{2T} + \frac{3eV\Theta}{T}\left[\frac{-c}{2} - \sqrt{-4a^2 + c^2}\cot h\left(\frac{\sqrt{-4a^2 + c^2}}{2}\delta^{\gamma}\right)\right] + f. \tag{65}$$

For Family 7, when $c^2 = 4ab$,

$$u_7(x,t) = \frac{3V(c\Theta - 1)}{2T} + \frac{3V\Theta}{T}\left[\frac{-2 + c\delta^\gamma}{2\delta^\gamma}\right],$$
$$v_7(x,t) = \frac{3eV(c\Theta - 1)}{2T} + \frac{3eV\Theta}{T}\left[\frac{-2 + c\delta^\gamma}{2\delta^\gamma}\right] + f. \tag{66}$$

For Family 8, when $ab < 0$, $c = 0$ and $b \neq 0$,

$$u_{8,1}(x,t) = \frac{-3V}{2T} - \frac{3bV\Theta}{T}\left[\sqrt{\frac{-a}{b}}\tan h\left(\sqrt{-ab}\delta^\gamma\right)\right],$$
$$u_{8,2}(x,t) = \frac{-3V}{2T} - \frac{3bV\Theta}{T}\left[\sqrt{\frac{-a}{b}}\cot h\left(\sqrt{-ab}\delta^\gamma\right)\right],$$
$$v_{8,1}(x,t) = \frac{-3eV}{2T} - \frac{3abV\Theta}{T}\left[\sqrt{\frac{-a}{b}}\tan h\left(\sqrt{-ab}\delta^\gamma\right)\right] + f,$$
$$v_{8,2}(x,t) = \frac{-3eV}{2T} - \frac{3abV\Theta}{T}\left[\sqrt{\frac{-a}{b}}\cot h\left(\sqrt{-ab}\delta^\gamma\right)\right] + f. \tag{67}$$

For Family 9, when $c = 0$ and $a = -b$,

$$u_9(x,t) = \frac{-3V}{2T} + \frac{3bV\Theta}{T}\left[\frac{1 + e^{-2b\delta^\gamma}}{-1 + e^{-2b\delta^\gamma}}\right],$$
$$v_9(x,t) = \frac{-3eV}{2T} + \frac{3ebV\Theta}{T}\left[\frac{1 + e^{-2b\delta^\gamma}}{-1 + e^{-2b\delta^\gamma}}\right] + f. \tag{68}$$

For Family 12, when $b = c = K$ and $a = 0$,

$$u_{12}(x,t) = \frac{3V(K\Theta - 1)}{2T} + \frac{3KV\Theta}{T}\left[\frac{e^{K\delta^\gamma}}{1 - e^{K\delta^\gamma}}\right],$$
$$v_{12}(x,t) = \frac{3eV(K\Theta - 1)}{2T} + \frac{3eKV\Theta}{T}\left[\frac{e^{K\delta^\gamma}}{1 - e^{K\delta^\gamma}}\right] + f. \tag{69}$$

For Family 13, when $c = a + b$,

$$u_{13}(x,t) = \frac{3V((a+b)\Theta - 1)}{2T} - \frac{3bV\Theta}{T}\left[\frac{1 - ae^{(a-b)\delta^\gamma}}{1 - be^{(a-b)\delta^\gamma}}\right],$$
$$v_{13}(x,t) = \frac{3eV((a+b)\Theta - 1)}{2T} - \frac{3ebV\Theta}{T}\left[\frac{1 - ae^{(a-b)\delta^\gamma}}{1 - be^{(a-b)\delta^\gamma}}\right] + f. \tag{70}$$

For Family 14, when $c = -(a + b)$,

$$u_{14}(x,t) = \frac{-3V((a+b)\Theta - 1)}{2T} + \frac{3bV\Theta}{T}\left[\frac{a - e^{(a-b)\delta^\gamma}}{b - e^{(a-b)\delta^\gamma}}\right],$$
$$v_{14}(x,t) = \frac{-3eV((a+b)\Theta - 1)}{2T} + \frac{3ebV\Theta}{T}\left[\frac{a - e^{(a-b)\delta^\gamma}}{b - e^{(a-b)\delta^\gamma}}\right] + f. \tag{71}$$

For Family 15, when $a = 0$,

$$u_{15}(x,t) = \frac{3V(c\Theta - 1)}{2T} + \frac{3bV\Theta}{T}\left[\frac{ce^{c\delta^\gamma}}{1 - be^{c\delta^\gamma}}\right],$$
$$v_{15}(x,t) = \frac{3eV(c\Theta - 1)}{2T} + \frac{3ebV\Theta}{T}\left[\frac{ce^{c\delta^\gamma}}{1 - be^{c\delta^\gamma}}\right] + f. \tag{72}$$

For Family 16, when $c = a = b \neq 0$,

$$u_{16}(x,t) = \frac{3V(c\Theta - 1)}{2T} + \frac{3bV\Theta}{2T}\left\{\sqrt{3}\tan\left(\frac{\sqrt{3}}{2}a\delta^\gamma\right) - 1\right\}\Bigg],$$
$$v_{16}(x,t) = \frac{3eV(c\Theta - 1)}{2T} + \frac{3ebV\Theta}{2T}\left\{\sqrt{3}\tan\left(\frac{\sqrt{3}}{2}a\delta^\gamma\right) - 1\right\}\Bigg] + f. \tag{73}$$

For Family 18, when $c = a = 0$,

$$u_{18}(x,t) = \frac{-3V}{2T} - \frac{3V\Theta}{T}\left[\frac{1}{\delta^\gamma}\right],$$
$$v_{18}(x,t) = \frac{-3eV}{2T} - \frac{3eV\Theta}{T}\left[\frac{1}{\delta^\gamma}\right] + f. \tag{74}$$

For Family 17, when $a = b$ and $c = 0$,

$$u_{19}(x,t) = \frac{-3V}{2T} + \frac{3bV\Theta}{T}[\tan(b\delta^\gamma)],$$
$$v_{19}(x,t) = \frac{-3eV}{2T} + \frac{3ebV\Theta}{T}[\tan(b\delta^\gamma)] + f. \tag{75}$$

5. Results and Discussion

This section covers the graphical interpretation of the results and the impact of the fractal parameter on them. Two powerful integration approaches, namely, semi-inverse scheme and AEM are used to extract soliton solutions of governing model. It has been established that the approaches currently provided for the double-chain DNA model, which were utilized to create closed-form exact results, are novel and distinct from those currently in use. The innovative solitonic solution structure and the new equations that yielded distinct types of solutions are the observable characteristics for finding solutions from the method outlined. Graphics that elaborate the various novel exact solitons in the forms of dynamics and nonlinear waves are presented for a physical description of the solutions that

have been achieved. The semi-inverse principle offers bright soliton solutions Equations (22), (23), (29), and (30) of the aforesaid system. The physical significance of these solitons is shown in terms of modulus of $u(x, t)$ by assigning particular values of free parameters. Equations (23) and (30) show the same graphical behavior with just translation given in Equation (4) as in the figures. In Figures 1 and 2, these solitons in the form of 3D plots for fractal dimension value $\gamma = 0.8$ and 2D graphs for $\gamma = 0.5,0.7,0.9$ are provided. Dual-wave periodic, dark, bright solitons are raised by executing AEM. The dynamics of DNA strands $u(x, t)$ and $v(x, t)$ are presented in Figures 3–12. 3D sketches for fractal value $\gamma = 0.3$ and 2D graphics for $\gamma = 0.5,0.7,0.9$ are provided. The fractal impact is displayed by the irregularity in the curves of solutions. A few representative solutions are graphically illustrated to consider the appropriate connotation of dual-wave behaviors of the DNA system. The propagation of solitons and collisions of dual-mode pulses are examined using graphs. It is important to note that the proposed schemes may be used to generate soliton solutions for any NLPDE.

6. Sensitivity Analysis

The sensitive analysis of the formulated soliton solutions is demonstrated in this section. There are several research publications on the methods and applications of sensitivity analysis of parameter uncertainty to mathematical problems. The goal of the study is to identify and classify the different types of uncertainty that can affect how well a mathematical equation or framework performs in relation to its inputs. Results are presented based on various parametric values, and sensitivity is investigated by taking into account how a little change in input can significantly alter output. A detailed analysis of Equation (9) is introduced in Figures 13 and 14.

7. Conclusion

In this manuscript, semi-inverse method and AEM have been successfully applied to the double-chain DNA model that is one of the interesting models of current biophysics since it is related to an organism's life. It is likely that the well-known cubic nonlinear Klein-Gordon equation is the linearly reduced model to (1). The fractal DNA system has a high influence because it is used to describe the nonlinear dynamics of DNA molecules. The dark, periodic, bright, and other soliton solutions are derived which may help biologists for physical simulation of suggested equations. It should be highlighted that our results are novel and different from those of earlier investigations [3, 9]. The semi-inverse scheme is a fascinating integration tool to deduce variational principles for various differential models, whereas AEM is compelling to derive a family of dual-wave solitons of any NLPDE. The relevant choices of parameters enable us to discuss fractal behavior of the system. Also, the nature of attained solutions is reviewed by their 3D and 2D graphics. By using various initial conditions, the system is subjected to sensitivity analysis, which is then visualized using graphs. The acquired effects might help spark original suggestions for future biological applications.

Data Availability

Data is available on request.

Conflicts of Interest

The authors have no conflict of interest regarding the publication of this paper.

Authors' Contributions

All authors have equal contribution on this paper.

Acknowledgments

The authors extend their appreciation to the Deanship of Scientific Research at King Khalid University, for funding this project under grant number R.G.P. 2/29/43. Emad E. Mahmoud acknowledges the Taif University Researchers Supporting Project number TURSP-2020/20, Taif University, Taif, Saudi Arabia.

References

[1] M. Aguero, M. Najera, and M. Carrillo, "Nonclassic solitonic structures in DNA's vibrational dynamics," *International Journal of Modern Physics B*, vol. 22, no. 16, pp. 2571–2582, 2008.

[2] G. Gaeta, "Results and limitations of the soliton theory of DNA transcription," *Journal of Biological Physics*, vol. 24, no. 2-4, pp. 81–96, 1999.

[3] A. R. Seadawy, M. Bilal, M. Younis, S. T. R. Rizvi, S. Althobaiti, and M. M. Makhlouf, "Analytical mathematical approaches for the double-chain model of DNA by a novel computational technique," *Chaos, Solitons and Fractals*, vol. 144, article 110669, 2021.

[4] Q. Xian-Min and L. Sen-Yue, "Exact solutions of nonlinear dynamics equation in a new double-chain model of DNA," *Communications in Theoretical Physics*, vol. 39, no. 4, pp. 501–505, 2003.

[5] L. V. Yakushevich, "Nonlinear DNA dynamics: a new model," *Physics Letters A*, vol. 136, no. 7-8, pp. 413–417, 1989.

[6] G. Gaeta, C. Reiss, M. Peyrard, and T. Dauxois, "Simple models of non-linearDNA dynamics," *Rivista del Nuovo cimento*, vol. 17, no. 4, pp. 1–48, 1994.

[7] M. Peyrard and A. R. Bishop, "Statistical mechanics of a nonlinear model for DNA denaturation," *Physical Review Letters*, vol. 62, pp. 2755–2758, 1989.

[8] S. M. Mabrouk, "Explicit solutions of double-chain DNA dynamical system in (2+1)- dimensions," *International Journal of Current Engineering and Technology*, vol. 9, 2019.

[9] Y. L. Ma and B. Q. Li, "Kraenkel-Manna-Merle saturated ferromagnetic system: Darboux transformation and loop-like soliton excitations," *Chaos Solitons And Fractals*, vol. 159, article 112179, 2022.

[10] S. Kumar and M. Niwas, "Exact closed-form solutions and dynamics of solitons for a (2+1)-dimensional universal hierarchy equation via Lie approach," *Pramana*, vol. 95, no. 4, p. 195, 2021.

[11] S. Kumar and A. Kumar, "Dynamical behaviors and abundant optical soliton solutions of the cold bosonic atoms in a zig-zag

optical lattice model using two integral schemes," *Mathematics and Computers in Simulation*, vol. 201, pp. 254–274, 2022.

[12] N. Raza, Z. Hassan, A. R. Butt, R. U. Rahman, A. H. Abdel-Aty, and M. Mahmoud, "New and more dual-mode solitary wave solutions for the Kraenkel–Manna–Merle system incorporating fractal effects," *Mathematical Methods in the Applied Sciences*, vol. 45, no. 5, pp. 2964–2983, 2022.

[13] Y. L. Ma and B. Q. Li, "Bifurcation solitons and breathers for the nonlocal Boussinesq equations," *Applied Mathematics Letters*, vol. 124, article 107677, 2022.

[14] L. Ouahid, M. A. Abdou, and S. Kumar, "Analytical soliton solutions for cold bosonic atoms (CBA) in a zigzag optical lattice model employing efficient methods," *Modern Physics Letters B*, vol. 36, no. 7, article 2150603, 2022.

[15] Y. L. Ma, A. M. Wazwaz, and B. Q. Li, "Two new types of nonlocal Boussinesq equations in water waves: bright and dark soliton solutions," *Chinese Journal of Physics*, vol. 77, p. 1782, 2022.

[16] A. A. Hendi, L. Ouahid, S. Kumar, S. Owyed, and M. A. Abdou, "Dynamical behaviors of various optical soliton solutions for the Fokas–Lenells equation," *Modern Physics Letters B*, vol. 35, no. 34, 2021.

[17] Y. L. Ma, A. M. Wazwaz, and B. Q. Li, "Novel bifurcation solitons for an extended Kadomtsev-Petviashvili equation in fluids," *Physics Letters A*, vol. 413, no. 3-4, article 127585, 2021.

[18] S. Arshed, N. Raza, N. Rahman, A. R. RU Butt, and W. H. Huang, "Sensitive behavior and optical solitons of complex fractional Ginzburg-Landau equation: a comparative paradigm," *Results in Physics*, vol. 28, article 104533, 2021.

[19] B. Q. Li, "New breather and multiple-wave soliton dynamics for generalized Vakhnenko–Parkes equation with variable coefficients," *Journal of Computational and Nonlinear Dynamics*, vol. 16, no. 9, article 091006, 2021.

[20] L. Ouahid, M. A. Abdou, S. Kumar, S. Owyed, and S. S. Ray, "A plentiful supply of soliton solutions for DNA Peyrard–Bishop equation by means of a new auxiliary equation strategy," *International Journal of Modern Physics B*, vol. 35, no. 26, article 2150265, 2021.

[21] Y. L. Ma, A. M. Wazwaz, and B. Q. Li, "A new (3+1)-dimensional Kadomtsev-Petviashvili equation and its integrability, multiple-solitons, breathers and lump waves," *Mathematics and Computers in Simulation*, vol. 187, pp. 505–519, 2021.

[22] S. Kumar and S. K. Dhiman, "Lie symmetry analysis, optimal system, exact solutions and dynamics of solitons of a ($$3+1$$)-dimensional generalised BKP-Boussinesq equation," *Pramana*, vol. 96, no. 1, 2022.

[23] Y. L. Ma, A. M. Wazwaz, and B. Q. Li, "New extended Kadomtsev–Petviashvili equation: multiple soliton solutions, breather, lump and interaction solutions," *Nonlinear Dynamics*, vol. 104, no. 2, pp. 1581–1594, 2021.

[24] S. Kumar and S. Rani, "Lie symmetry reductions and dynamics of soliton solutions of (2+1)-dimensional Pavlov equation," *Pramana*, vol. 94, no. 1, p. 328, 2020.

[25] B. Q. Li and Y. L. Ma, "Interaction dynamics of hybrid solitons and breathers for extended generalization of Vakhnenko equation," *Nonlinear Dynamics*, vol. 102, no. 3, pp. 1787–1799, 2020.

[26] S. Kumar, S. K. Dhiman, and A. Chauhan, "Symmetry reductions, generalized solutions and dynamics of wave profiles for the (2+1)-dimensional system of Broer-Kaup-Kupershmidt (BKK) equations," *Mathematics and Computers in Simulation*, vol. 196, pp. 319–335, 2022.

[27] B. Q. Li and Y. L. Ma, "Extended generalized Darboux transformation to hybrid rogue wave and breather solutions for a nonlinear Schrodinger equation," *Applied Mathematics and Computation*, vol. 386, article 125469, 2020.

[28] S. Kumar, M. Kumar, and D. Kumar, "Computational soliton solutions to (2+1)-dimensional Pavlov equation using lie symmetry approach," *Pramana*, vol. 94, no. 1, p. 28, 2020.

[29] N. Raza, A. Jhangeer, R. U. Rahman, A. R. Butt, and Y. M. Chu, "Sensitive visualization of the fractional Wazwaz-Benjamin-Bona-Mahony equation with fractional derivatives: a comparative analysis," *Results in Physics*, vol. 25, article 104171, 2021.

[30] A. Jhangeer, W. A. Faridi, M. I. Asjad, and A. Akgül, "Analytical study of soliton solutions for an improved perturbed Schrodinger equation with Kerr law non-linearity in nonlinear optics by an expansion algorithm," *Partial Differential Equations in Applied Mathematics*, vol. 4, article 100102, 2021.

[31] J. Rao, D. Mihalache, J. He, and Y. Cheng, "Dynamics of general higher-order rogue waves in the two-component nonlinear Schrodinger equation coupled to the Boussinesq equation," *Communications in Nonlinear Science and Numerical Simulation*, vol. 110, article 106382, 2022.

[32] A. Bekir and E. H. M. Zahran, "Painlevé approach and its applications to get new exact solutions of three biological models instead of its numerical solutions," *International Journal of Modern Physics B*, vol. 34, no. 29, article 2050270, 2020.

[33] Y. Khan, "Fractal modification of complex Ginzburg-Landau model arising in the oscillating phenomena," *Results in Physics*, vol. 18, article 103324, 2020.

[34] C. H. He, Y. Shen, F. Y. Ji, and J. H. He, "Taylor series solution for fractal Bratu-Type equation arising in electrospinning process," *Fractals*, vol. 28, no. 1, article 2050011, 2020.

[35] N. Raza and A. Javid, "Generalization of optical solitons with dual dispersion in the presence of Kerr and quadratic-cubic law nonlinearities," *Modern Physics Letters B*, vol. 33, no. 1, article 1850427, 2019.

[36] Z. Hassan, N. Raza, and J. F. Gomez-Aguilar, "Novel optical solitons to the perturbed Gerdjikov–Ivanov equation via collective variables," *Optical and Quantum Electronics*, vol. 53, no. 8, pp. 1–19, 2021.

[37] K. K. Ali, M. S. Osman, and M. Abdel-Aty, "New optical solitary wave solutions of Fokas-Lenells equation in optical fiber via Sine-Gordon expansion method," *Alexandria Engineering Journal*, vol. 59, no. 3, pp. 1191–1196, 2020.

[38] N. Raza, M. Abdullah, A. R. Butt, I. G. Murtaza, and S. Sial, "New exact periodic elliptic wave solutions for extended quantum Zakharov-Kuznetsov equation," *Optical and Quantum Electronics*, vol. 50, no. 4, 2018.

[39] M. S. Osman, "Multi-soliton rational solutions for some nonlinear evolution equations," *Physics*, vol. 14, no. 1, pp. 26–36, 2016.

[40] A. R. Seadawy, M. Iqbal, and D. Lu, "Propagation of kink and anti-kink wave solitons for the nonlinear damped modified Korteweg-de Vries equation arising in ion-acoustic wave in an unmagnetized collisional dusty plasma," *Physica A*, vol. 544, article 123560, 2020.

[41] A. Jhangeer, H. Almusawa, and R. U. Rahman, "Fractional derivative-based performance analysis to Caudrey-Dodd-Gibbon- Sawada-Kotera equation," *Results in Physics*, vol. 36, article 105356, 2022.

[42] N. Raza, A. Jhangeer, H. Rezazadeh, and A. Bekir, "Explicit solutions of the (2 + 1)-dimensional Hirota–Maccari system

arising in nonlinear optics," *International Journal of Modern Physics B*, vol. 33, no. 30, article 1950360, 2019.

[43] M. I. Asjad, W. A. Faridi, A. Jhangeer, H. Ahmad, S. Abdel-Khalek, and N. Alshehri, "Propagation of some new traveling wave patterns of the double dispersive equation," *Open Physics*, vol. 20, no. 1, pp. 130–141, 2022.

[44] J. H. He, "Variational principles for some nonlinear partial differential equations with variable coefficients," *Chaos, Solitons and Fractals*, vol. 19, no. 4, pp. 847–851, 2004.

[45] J. H. He, "Some asymptotic methods for strongly nonlinear equations," *International Journal of Modern Physics B*, vol. 20, no. 10, pp. 1141–1199, 2006.

[46] A. Biswas, D. Milovic, M. Savescu, M. F. Mahmood, and K. R. Khan, "Optical soliton perturbation in nanofibers with improved nonlinear Schrödinger's equation by semi-inverse variational principle," *Journal of Nonlinear Optical Physics and Materials*, vol. 21, no. 4, article 1250054, 2012.

[47] J. Zhang, "Variational approach to solitary wave solution of the generalized Zakharov equation," *Computers and Mathematics with Applications*, vol. 54, no. 7-8, pp. 1043–1046, 2007.

[48] D. Kumar, C. Park, N. Tamanna, G. C. Paul, and M. S. Osman, "Dynamics of two-mode Sawada-Kotera equation: mathematical and graphical analysis of its dual-wave solutions," *Results in Physics*, vol. 19, article 103581, 2020.

[49] H. Rezazadeh, A. Korkmaz, M. Eslami, and S. M. Mirhosseini-Alizamini, "A large family of optical solutions to Kundu–Eckhaus model by a new auxiliary equation method," *Optical and Quantum Electronics*, vol. 51, no. 3, 2019.

[50] J. H. He, "A fractal variational theory for one-dimensional compressible flow in a microgravity space," *Fractals*, vol. 28, no. 2, article 2050024, 2020.

[51] J. H. He, "Fractal calculus and its geometrical explanation," *Results in Physics*, vol. 10, pp. 272–276, 2018.